Egyptian Geophysical Society
EGS Journal, Vol. 11, No. 1, 93-104 (2013)

CHARACTERIZATION OF THE FRACTUR-FAULT SYSTEM IN SOUTH SINAI-EGYPT, USING GEOPHYSICAL INVESTIGATIONS

M.M. Mekkawi*, A.M. Abed and M.A. Hafez

National Research Institue of Astronomy and Geophysics,
*(NRIAG-11421 HELWAN), Egypt. * E-mail; mekkawi05@yahoo.com*

تمييز الفوالق والشقوق فى جنوب سيناء بأستخدام الطرق الجيوفيزيقية.

الخلاصة: تقع منطقة الدراسة فى جنوب سيناء وتتركز فيها كثير من المدن السياحية ومنها مدينة شرم الشيخ التى تعتبر من أهم الأماكن السياحية فى مصر. وتعتبر دراسة الفوالق النشطة فى جنوب سيناء بهدف التحديد الدقيق للاجزاءالمتصدعة من حدوث الزلازل. لتوضيح هذه الأجزاء فى التراكيب تحت سطحية، استخدمنا المعلومات الجيولوجية المتاحة وتحليل الزلازل الت حدثت فى المنطقة والمعلومات المغناطيسية الأرضية وكذلك الموجات الرادارية الأختراقية. وأوضحت الدراسات أن الزلازل تتراكز فى ثلاث مناطق هى البحر الاحمر وخليج العقبة وخليج السويس. وان معدل الزلازل وسلوكها واعماقها وكذلك تركيزها تختلف. وان التراكيب الجيولوجية والفوالق التى اوضحتها الدراسات المغناطيسية لها اتجاهات فى الشمال الشرقى– الجنوب الغربى و الشمال الغربى–والجنوب الشرقى وكذلك الشرقى–الغربى. ام الدراسات الرادارية اوضحت التراكيب الجيولوجية القريبة من السطح وكثيير من الفوالق والشقوق. ولابد الأخذ فى الاعتبار كل هذة الفوالق والشقوق عند بناء القرى السياحية فى شرم الشيخ لانها تقع عند التقاءات البحر الاحمر وخليج العقبة وخليج السويس.

ABSTRACT: *Studying the active faults in South Sinai aims to accurately locate potential areas of rupture as a part of seismic hazard evaluation. In order to describe the faults system characteristics in south Sinai, the subsurface structures have been investigated based on the geological, ground penetrating radar, seismicity and land magnetic data. Ground-Penetrating Radar (GPR) survey has been conducted to image near surface sedimentary environments. Sites of investigation are mainly based on the known and unknown trends of faults. The result of GPR imaging shows that, a lot of fractures and sinkholes are associated with the fault system in Sharm El-Sheikh which could be a risk for the buildings. It reveals the branching geometry of faults and the precise location within 1 m. The magnetic data reveal that, the area is affected by a set of faults trending mainly in the NNE-SSW, NW-SE, E-W and N-S directions. Also, the basement structural trends are controlled mainly by these predominant faults. Furthermore, the seismicity is concentrating in three seismic segments (northern part of Red sea, Gulf of Aqaba and Gulf of Suez). These seismic zones behave differently over the time and space domains, as indicated by the seismic rate, depth migration, b-value and special clustering. This integration demonstrates the seismically active segments, which can be related to the tectonic movements in the Gulf of Aqaba and probably generated relative large movement rates in the future, which must be considered in the engineering designs and constructions.*

Keywords: *South Sinai seismicity, magnetic data, Ground Penetrating Radar and Fracture fault system.*

INTRODUCTION

The Sinai Peninsula is rich in the natural and mineral resources, such as, Manganese (*Umm Bougma*), Coal (*Gebel Maghara*), *80 %* of the oil production in Egypt (*Gulf of Suez*), Copper and Uranium (*Ashami, 2003*). It has recognized as a part of the African plate (*sub-plate*) located at the triple junction of the northern part of the Red Sea, the Gulf of Suez and Aqaba-Levant transform fault *(Ben-Manhem et al., 1976).* Several geological and seismological investigations assert that the Aqaba-Levant transform fault displays a higher rate of motion (9 mm/y) than the Gulf of Suez (3mm/y). At present, some extensions are still recognized, but with a low deformation rate (*Steckler et al., 1988 and El Fiky, 2005 and Rielinger et al 2006).*

On the east, the Gulf of Aqaba exhibits a well-defined plate boundary and is characterized by dominant left-lateral motion with small component of extension along the N*NE-SSW* fault. It is built of two phases of *NNE-SSW* pull-apart basins, *N-S* to *NNE-SSW* striking fault. It represents the southern part of the Red Sea transform fault, which runs from the northern end of the spreading to reach the continental collision of the Zagros-Taurus zone *(Ben Avraham 1985; Abdel-Fattah et al 2006*; *and Baer et al 2008)*. The Gulf of Suez region has long been recognized one of the best examples of long-axis segmentation with different dip polarities. It is suggested interaction between extensional tectonics and sedimentations. It is remarkable non-volcanic with only a few late pre-rift to early syn-rift basic dykes and isolated basaltic features *(Colleta et al., 1988; Patton et al 1994; Sharp et al., 2000 and Rabeh et al., 2009)*.

Recent geophysical studies in the active regions of south Sinai are mentioned by many authors *(McClusky 2000; Shamir 2003; Awad et al 2009 and Khafef & El-Khoudary 2011)*. They considered that the study area is a part of the Tertiary Cratonic rift between North Africa (*Nubian Plate*) and Arabian Peninsula (*Arabian Plate*). On the south part, the Red Sea zone is subjected to pull apart motion affected by the rotation between Africa and Arabian plates.

The area under study (*Figure 1*) is approximately 225 km long (north-south) and 275 km wide (west-east). The surface area has an extension of 61875 km^2 between latitudes (*28°00'-30 00'N*) and longitudes (*32°00'-35°00'E*). It is characterized by historical locations (Route of holy family and Saint Catharine church). South Sinai has a unique situation view (Ras Sudr, Tur, Ras Mohamed, Sharm El-Sheikh Dahab, Nuweiba and Taba). These places are the leading seashore resorts on the Gulf of Aqaba and Gulf of Suez and have attracted the Egyptian and foreign visitors.

Both the geological and geophysical tools (GPR, land magnetic and seismicity analysis) are used in order to delineate the fracture fault system (*triple junctions*) generating earthquakes, that affecting the touristic resorts in south Sinai. The separation of the two continents caused the form and geographical shape (*triangular*). The tectonic movements rates probably generate large earthquakes (*Aqaba earthquake, 1995, M=7.2*), which must be considered in the engineering designs and constructions in future.

Geologic and tectonic settings:

The surface rock units of South Sinai range from the Precambrian (basement) rocks to the Quaternary deposits *(Figure 2)*. The basement rocks are located in the southern part, the Paleozoic rocks in the middle part, while the Mesozoic occupies the eastern and western parts in the studied area. Sharm El-Sheikh area has the following geological periods: Precambrian, lower Miocene, Cretaceous, Pliocene and Quaternary (*EGSMA, 1994*). The rocks are exposed north and west of Sharm El-Sheikh area forming the northern part of the rocky land at the coastal plain. These outcrops are composed mainly of alternate beds of marl and sandstones, with fossilleferous carbonate beds in the lower part. Pliocene rocks are exposed along the coastal plain from *Ras Mohammed* (in the south) to *Ras Nusrani*, forming the rocky lands of the coast. They comprise dark colored conglomerates, that alternate with sandstone beds. Quaternary deposits are made up of coralline limestone, wadi and alluvial deposits (*Omara et. al, 1959*).

Structurally, both the basement rocks and the thin sedimentary cover exhibit a large number of surface tectonic elements, varying lengths and trends *(Figure 3)*. Regional study of the linear features such as faults, joints, folds, dikes, crustal fractures and lithological contacts, using the aerial photographs and particular satellite images *(Google Earth website)* has made important advances in the geological research. Recognition of lineaments has been used for investigating active fault patterns in the areas of difficult accessibility. The predominant fault direction systems are: *NW-SE* (Gulf of Suez), *NNE-SSW (Gulf of Aqaba), N-S* (East Africa Rift System) and *E-W* (Mediterranean Sea), as shown by *(Neev, 1975, Agah, 1981 and Said, 1990).*

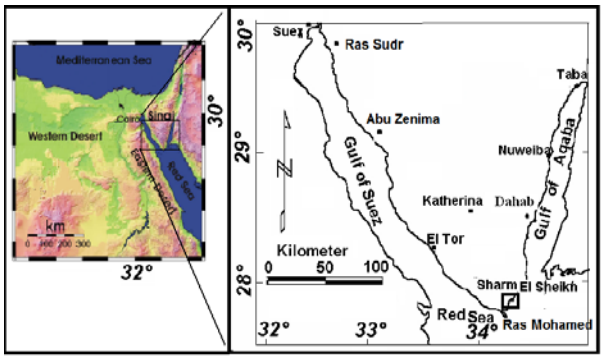

Figure 1: Location map of South Sinai area and main touristic resorts along its two branches (Gulf of Suez & Gulf of Aqaba).

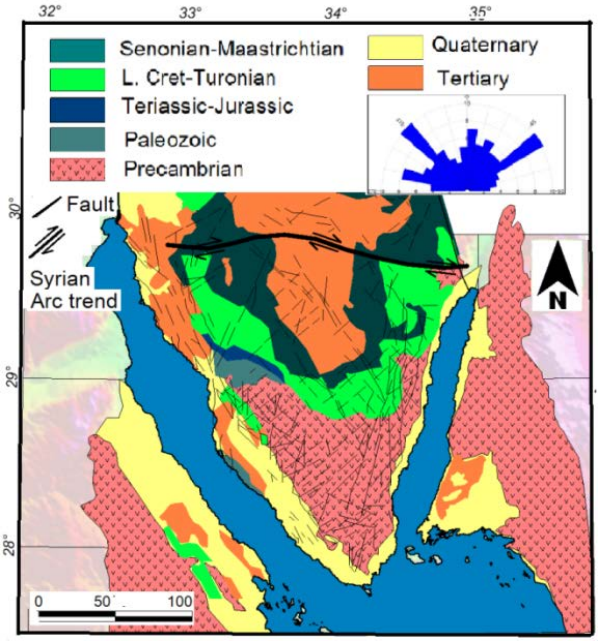

Figure 2: Geologic map of South Sinai area (Neev, 1975 and Agah, 1981). The rose diagram shows the main trends of the surface geologic faults in South Sinai Peninsula.

In Egypt, moderate intra-plate earthquakes of magnitude (*M<6*) are commonly occurred in the upper crust. The (*M=5.2*) Aswan earthquake of 14 November 1981 called the attention to the importance of earthquake monitoring in the High Dam area and risk studies in the country. In addition, Dahshour earthquake of October 1992 (*M=5.9*) which damaged over 1000 schools, killed and injured over 7000 people. In 1969 and 1995, two earthquakes occurred along the northern Red Sea and Gulf of Aqaba (*M= 6.9 and 7.2, respectively*), addition to many events with (*M>5*).

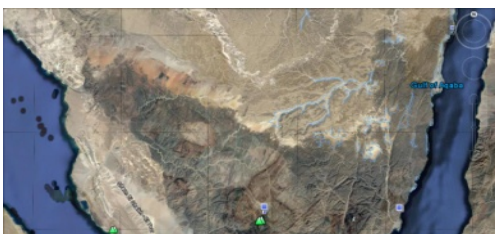

It were produced by sudden slips along major active faults with offset of tens of meters taken place in a few seconds and caused extensive damage. Already small and moderate earthquakes provide clues to the locations of active faults.

Seismicity of South Sinai:

Seismic hazard assessment in Egypt was done by *(El-sayed et al., 2001; El-Hefnawy et al., 2006; Korrat et. al, 2006; Fergani, 2007 and Abdel Rahman, 2009)*, using the spatial distribution of recorded earthquakes *(Figure 4)* to identify the major seismic zones and seismogenic zones with common focal mechanisms. Lines denote the major tectonic elements and Seismogenic zones with focal mechanisms in Egypt and its vicinity: **1** Gulf of Aqaba-Levant; **2** Northern Red Sea–Gulf of Suez; **3** Suez–Cairo–Alexandria; **4** Eastern Mediterranean–Cairo–Fayoum; **5** Mediterranean costal; **6** Cyprus; **7** Crete; **8** Gilf el-keber; **9** Aswan and **10** Qena zone.

Seismic activities are mainly occurred along the borders of Sinai (*sub-plate*), in the southern part of the Gulf of Suez and along the Aqaba-Levant fault system. *Awad et al.(2009)* have demonstrated seismic sources (seismic segments) within the South Sinai block as follow: *NE-SW, NW-SE and NNW-SSE*. Seismicity distribution indicates that, the earthquakes in zones occur due to the tectonic movements. The Arabian plate moves northward relative to Africa (*Ben-Menahem et al, 1967*). Focal mechanisms are analyzed by *(El-Fiky 2005).* The Gulf of Suez motion with extensional features and the Aqaba-Levant fault system have both left-lateral strike-slip and extensional motions. *Badawi and Horvath (1999)* located historical events in that area, such as the 18 March 1068 (*Levant Fault*); 20 May 1202 (*Dead Sea*) and 11 July 1879 (*Gulf of Suez*).

The South Sinai Seismic Catalog:

In the present work the South Sinai catalogue is analyzed using *ZMAP-6.0 software (Weimer, 2001)* in order to correlate between the seismicity occurred and subsurface structures. The hazard reduction, from the natural disasters of earthquakes, becomes a primary concern in the South Sinai touristic places, which are moving rapidly towards huge investments and development. To evaluate the seismicity patterns in time and space domains, we used statistical techniques, such as average spatial behavior, *b*-value change over time.

The seismic data are continuously collected from the seismic stations at the recording center in the Egyptian National Seismic Network (*ENSN*) since 1997. The data catalog has been recorded (*1983-2010*) by at least four stations and contains about 7865 events (0.5<M<7.2). Using the Hypo71 code *(Lee, 1990)*, estimates of the locations errors are in the order of a few kilometers. The seismicity is concentrated along the borders of South Sinai, particularly at the Aqaba-Levant transform fault, Gulf of Suez and northern part of Red sea *(Figure 5).* Sharm El-Sheikh city lies at the active triple junction zone. It is characterized by fault segments, cross faults and shallow earthquakes (0.1<depth>24 km). A robust decrease in the average depths (*Figure 6*) is resolved for the shallow events during the 1983–1994 period, with a slower decreasing rate in the 1985–2010 period. The average depths for all the events decrease until 1995-1996 period. The observed mean depths oscillate (anomaly) in shallow and all earthquakes are driven before 1995 earthquake (*M=7.2*).

Figure (7) shows the cumulative events rate, that suggests a roughly increase in seismicity rate events before the Aqaba earthquake, *1995 (M=7.2).* An Intensive earthquake swarms occurred during the period *(Jan. 1983-March 1983), (Aug. 1993-Feb. 1994), (Nov. 1995-March 1996) and (May-2003-July 2003).*

In Figure (8), The Gutenberg–Richter distribution, in the range 2.3>*M*< 4.8, is recovered for the Suth Sinai seismicity and using the evolution of the *b*-values:

$$b = ln(10)\,(M_{avg} - M_{min}) \qquad (1)$$

where: M_{avg} is the average magnitude and M_{min}=1.8, the smallest considered magnitude. The *b*-values are estimated by using the maximum likelihood method of *Aki (1965).* Estimates of the *b*-values from maximum likelihood are 0.56 +/- 0.04 for all events. These values argue for a change in the *b*-values with time. The *b*-value remains roughly constant (1983-1990), but decreases and oscillate is increasing till period 2010.

The magnetic data:

The available land magnetic data of South Sinai which was compiled by (*Ismail et al. 2001*) will be re-interpreted using the Tilt Derivative method *(TDR)* in order to delineate the subsurface structures, linking it with the seismicity and trace the seismic hazard zones in the region. The *TDR* filter has been applied to the *RTP* land magnetic anomaly map *(Figure 9)*, from which the locations of the contacts or faults can be traced easily on the map.The *TDR* and its total horizontal derivative are useful for mapping the shallow basement structures. This filter is estimated by dividing the vertical derivative by the total horizontal derivative *(Verduzco, 2004)*, as follow:

$$TDR = \arctan(VDR / THDR) \qquad (2)$$

where: *VDR and THDR are the first vertical derivative and* the total horizontal derivatives of the magnetic data, respectively:

$$VDR = dT/dz \qquad (3)$$

$$THDR = sqrt\,((dT/dx)^2 + (dT/dy)^2) \qquad (4)$$

The most advantage of the *TDR* is that, its zero contour line is on or close to the fault/contact location (*Aboud et al., 2011*). *Figure (10)* shows the magnetic data with the zero contour line (*yellow colour*). *It* enhances the magnetic trends indicating that, the major structures of the area are *NW-SE* (Gulf of Suez trend) and *NNE-SSW* (Gulf of Aqaba trend) directions.

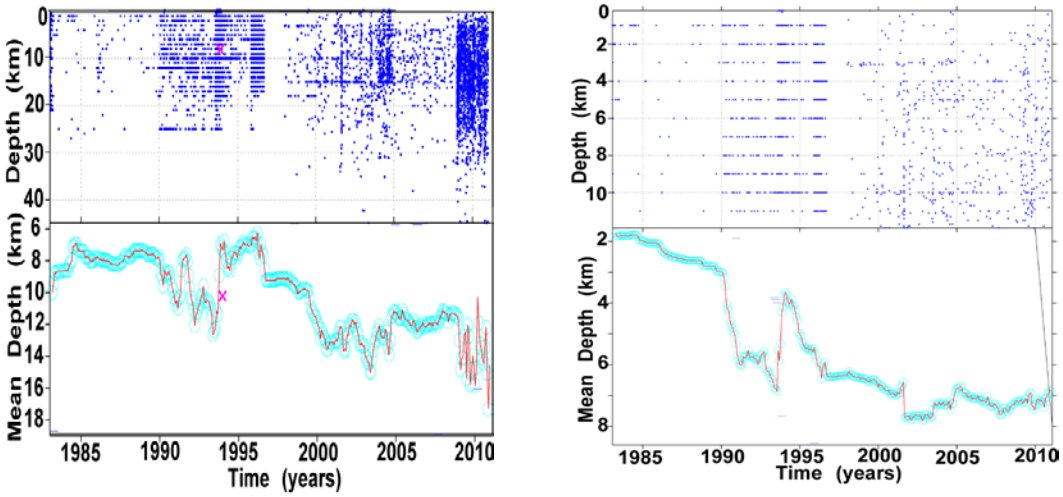

Figure 6: Time-depth histogram of south Sinai catalog for all focal depth (left) and shallow (right) in the period (1983-2010).

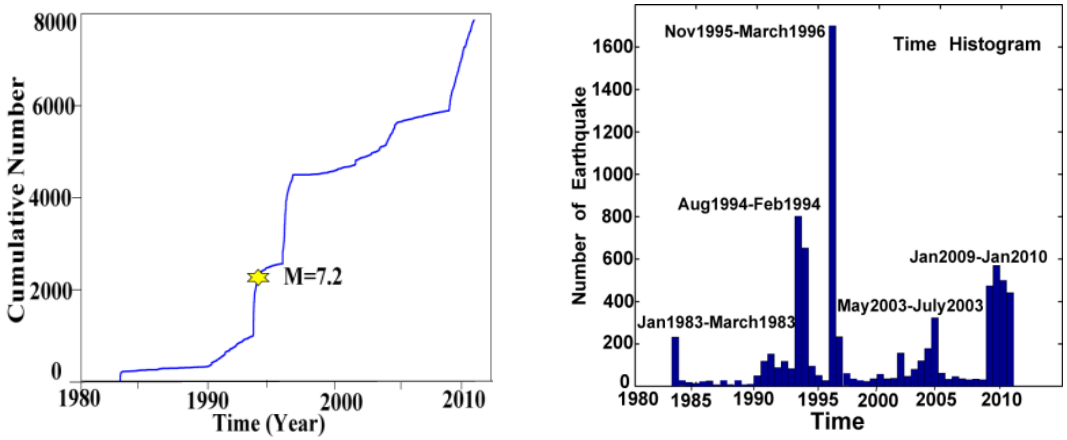

Figure 7: The Cumulative number of Earthquakes over time (left) of south Sinai Catalog and earthquakes swarms for the period (1983-2010).

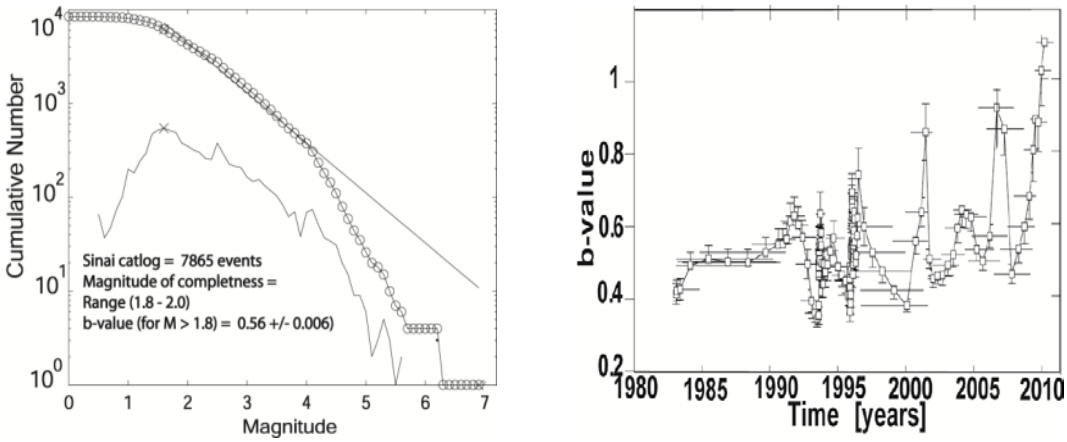

Figure 8: Magnitude–frequency distribution for south Sinai catalog using maximum likelihood (left) and change of the b-value with time (right).

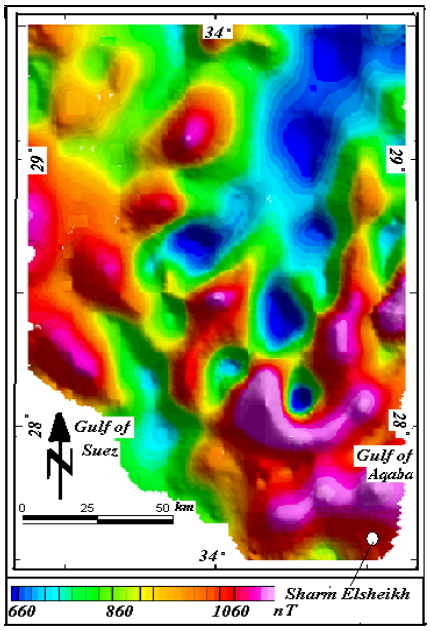

Figure 9: RTP land magnetic map of south Sinai area (After, Ismail et al., 2001).

Also, there are some other trends in the area; NE-SW (Syrian arc trend), *E-W* (Mediterranean trend) and *N-S* (East Africa rift) directions. However, the surface geologic map has evidences for faults (*Figure 2*). Also, some subsurface faults can be traced from the *TDR* map crossing the Sharm El-Sheikh and trending in the NE-SW direction. Moreover, the locations of the earthquakes in the area were obtained from the *ENSN-Egypt*. These locations (*crosses on figure 10*) are projected on the *TDR* magnetic map, which indicate that, some earthquakes occurred along the active faults and other close to the zero contour line.

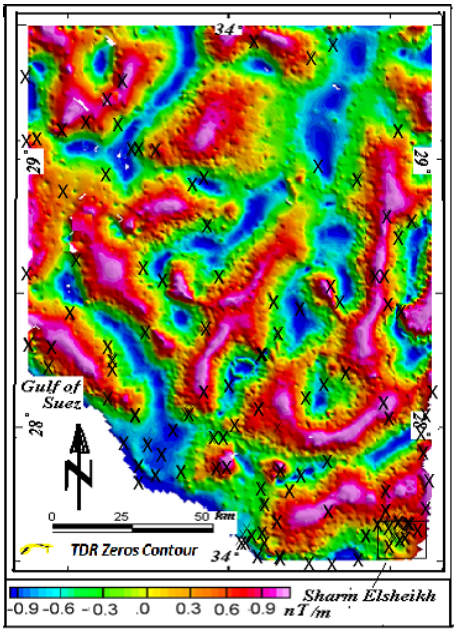

Figure 10: TDR magnetic anomaly map of south Sinai. Yellow color indicates zeros contour (active faults) and crosses seismicity distribution for M>2.

Tracing the zero contour line of the TDR map resulted in delineating the shallow basement structures of the area and drawing the faults that characterized the area as shown *in figure (11).* From these results, it could be concluded that along the zero contour lines (faults and fractures) of the TDR map, where is a possibility for future earthquakes. This result helps the decision makers to choose the best sites for constructions.

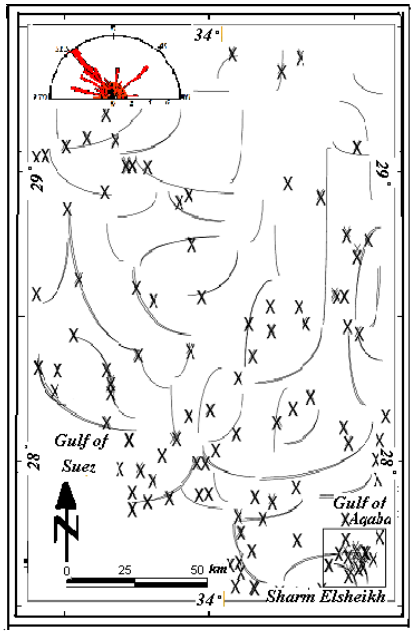

Figure 11: Interpreted active faults from TDR magnetic filter (solid lines) and Earthquake distribution (for M >2) around Sharm El-Sheikh.

Ground penetrating radar (GPR):

The *GPR* survey is a useful method for shallow engineering investigations (*Morey, 1974; Ulriksen, 1982; Ballard, 1983; Olhoeft, 1984, 1988*). The most important advantage of GPR is that no physical contact between the transmitter and receiver antenna and the subsoil is necessary. The primary disadvantage is its extremely site specific applicability (*Wadhwa, et al., 2008).* Minor structures and buried sinkholes were also mapped using the *GPR* in Egypt and Jordan, respectively, by *El-Behiry and Hanafy (2000) and Batayneh et al. (2002).El-Qady et. al (2005)* used the integrated two-dimensional resistivity tomography and Ground penetrating radar to image the subsurface cavities in Al-Amal city, Cairo-Egypt. Recently, *Wadhwa, et al. (2008)* employs GPR and electrical resistivity imaging to get the exact dimensions of the exposed cavities, as well as to delineate the subsurface cavities.

The GPR survey uses pulses of Electromagnetic (*EM*) radio waves directed down into the soil profile from a transmitting antenna, in order to investigate subterranean features. When discontinuities are encountered some of these radio waves are reflected back towards the surface, while other waves travel further down into the soil profile until they meet other

discontinuities. At the surface, a receiving antenna measures the reflected waves. By measuring the time taken between the emission of the radar pulse and the reception back at the antenna, it is possible to measure the depth of a discontinuity in the soil profile. Within a floodplain context, the boundaries between different geomorphological units will be seen as discontinuities, due to their different physical properties.

The GPR survey has been conducted in a site close to active faults, that cutting the land surface in Sharm El-Sheikh, in order to study the serious geo-hazard. The numbers of GPR profiles are 51 with *1m* spacing (*Figure 12*). In figure (12) the GPR profile spacing is 5 m to be readable. The measurements have been conducted using a *SIR 3000, GSSI*, Inc. equipped with 270 MHz antenna. The data have been processed using *Reflex software* (*Sandmeier, 2010*). It is important to recognize that velocity measurements at a site are valid only for the GPR data collected when the tests are performed. The velocity of radar waves at site can vary dramatically with the seasons. Changes in soil and sediment moisture can also occur rapidly, even as a survey is carried out, due to torrential rainfall or flooding.

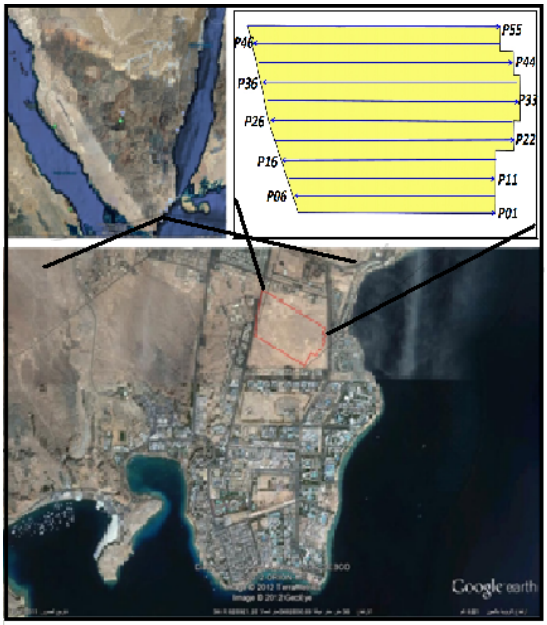

Figure 12: Location map and sketch diagram shows the GPR profiles distribution on the Sharm El-Sheikh site.

For example, velocity tests performed at Ceren site during the rainy season yielded a RDP of 12 (velocity of 8.7 cm/ns, for the volcanic overburden material *(Doolittle and Miller, 1992),* whereas tests performed in same area at the end of a 6 month dry season measured a RDP of about 5 or velocity of 13.4 cm/nS (Conyers, 1995). in this site the velocity have been determined through CMP measurement carried out using a bi static antenna of *100 MHz.* The semblance analyses have been used. Its aim is to find the velocity and the travel time for which the reflecting energy of a reflected wave in multi-offset measurements collapses to a point. This was done with the help of semblance plot, which is constructed by recalculating the arrival times of the CMP for a range of velocities and summing the normalized energy for each arrival time for each velocity. High values in the semblance plot indicate that the reflected waves at that particular arrival time are well described by that particular velocity. We conclude that the average ground-wave velocity from the GPR common-midpoint surveys is *0.1 m/ns.* This value, although approximate, is used to convert the two-way travel times to depths in the GPR sections. the semblance analysis is shown in *(Figure 13).* Other GPR processing includes dewowing and low-pass filtering of the GPR signals to remove the high-frequency system and cable noises. The *GPR* section along profile *P36* is given here to illustrate the processing effect on the raw data, that was acquired in the field, and also shows the stratigraphic conformity. *Figure (13)* represents the row data, while (*Figure 14*) represents the processed data.

The inspection of GPR profile P36 shows, a trough-like reflection, or coalescing series of diffractions, is centered at about 15 m , 30 m and 55 m along the line, extending from a two-way travel time of about 20 ns to 40 ns (1-2 m). This feature is interpreted to be a filled sinkhole at the bedrock surface, the GPR section also reveals possible layering in the filling materials, possibly representing repeated collapse and infilling. Signal penetration is relatively good along this line, so these filling materials are probably composed largely of sand and gravel, sediments with high hydraulic conductivity.

The results of *GPR* survey proved to be a successful method in imaging the subsurface structures of the underlying layers. The *GPR* sections (*Figures 16, 17 and 18*) reveal that, the subsurface of the site is composed of surface loose sandy layer extend to a depth of 0.5 m followed by a compact sand layer which reaches a depth ranging from 2 to 2.2 m. Finally the bed rock of massive limestone extends to the end of the section. Moreover, the results from GPR survey produced the most conclusive evidence as to the location of the air filled voids. The maximum depth of penetration was ***8 m*** along the traverse lines, which enables mapping features at a depth of about 8 meters.

GPR time slices:

Time slice maps are built averaging the amplitude (or the square amplitude) of the radar signal within consecutive time windows of width Δt. Sometimes, a particular complex-trace attribute, the instantaneous amplitude or envelope (*modulus of the Hilbert transform*) is used instead. Being a measure for reflectivity strength, it helps to evidence high amplitude anomalies. Previous spatial averaging is also useful to reduce small-scale heterogeneity noises. Finally, the data are interpolated and gridded on a regular mesh. Selecting the various parameters involved, in particular the width of the slice, Δt, is crucial.

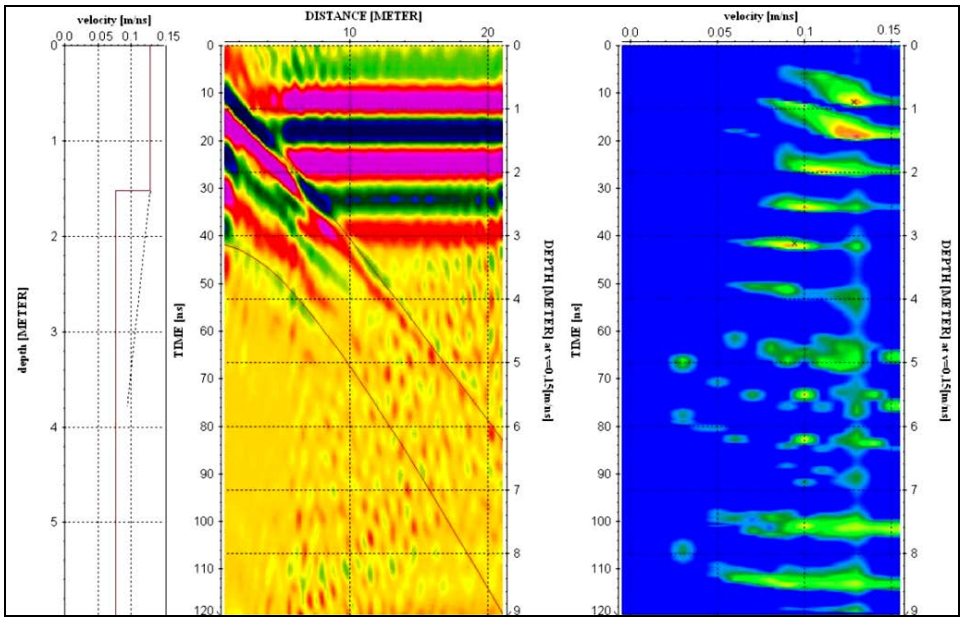

Figure 13: Semplance analysis of CMP data.

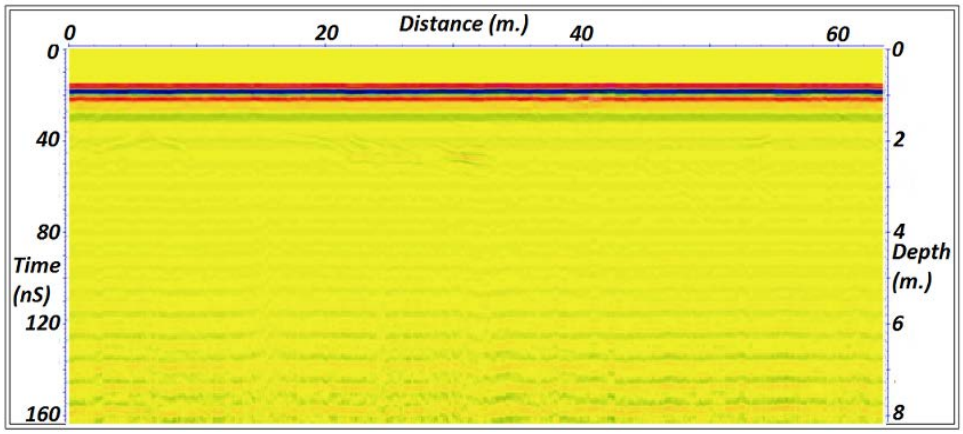

Figure 14: Row data of GPR section along profile P36.

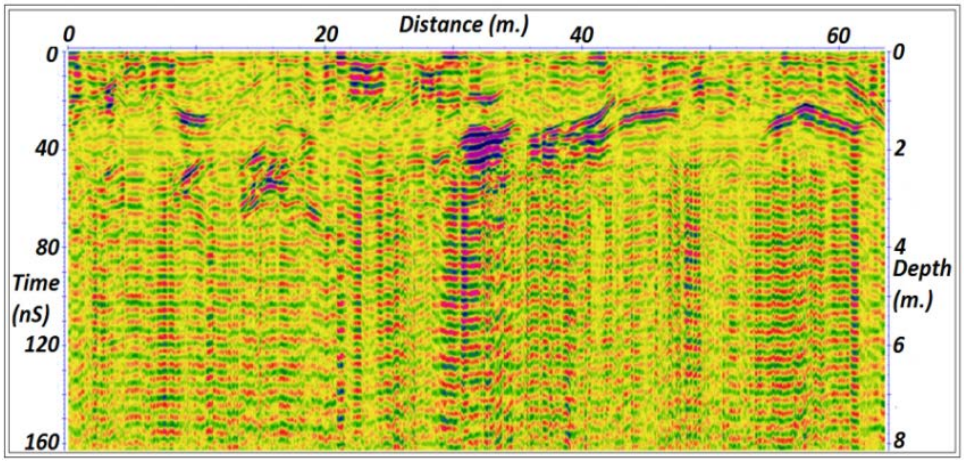

Figure 15: Processed data of GPR section along profile P36.

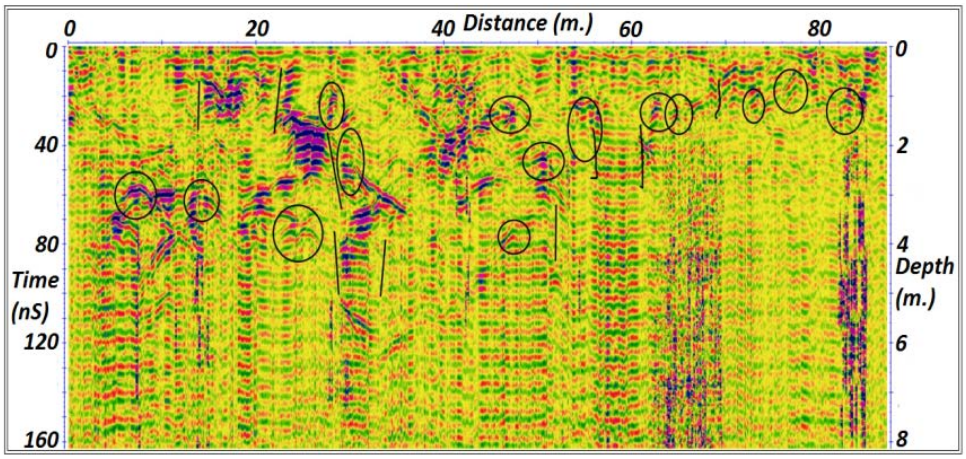

Figure 16: 2-D GPR section along profile P37 shows air filled voids and fractures.

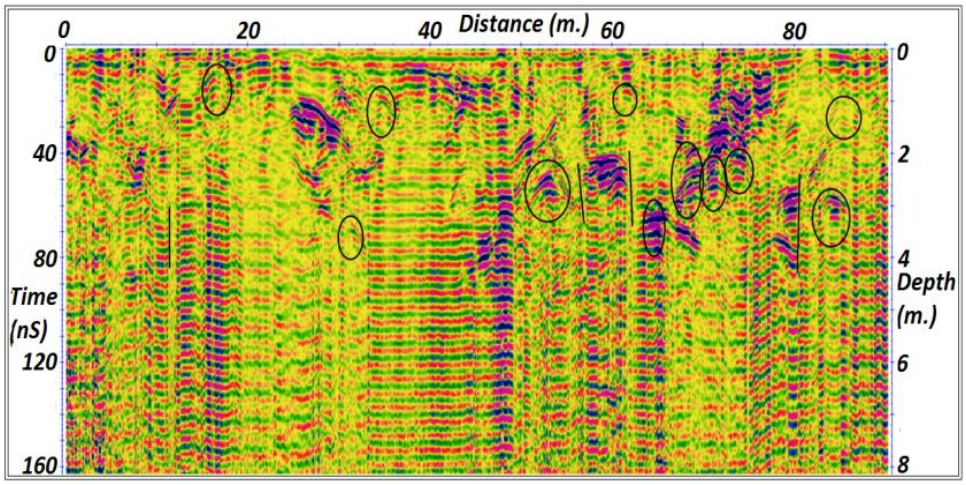

Figure 17: 2-D GPR section along profile P38 shows filled voids and fracture system.

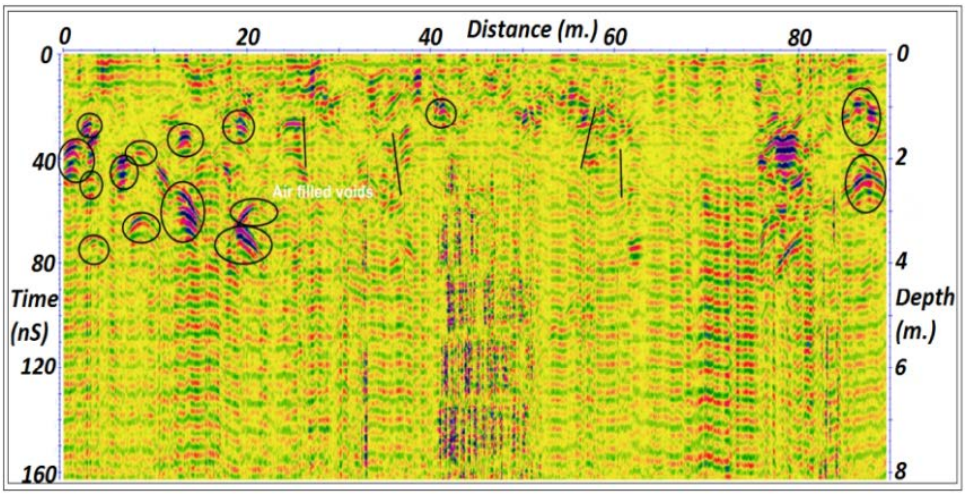

Figure 18: 2-D GPR section along profile P39 shows air filled voids with fracture system.

Typically Δt must be of the order of the dominant period, but different widths can be used to enhance particular features. Time slicing is attempted to image the subsurface setup by providing a plan-metric vision of the buried bodies.

Before slices construction is applied, the envelope of the C-scan in the 3D image is computed. This is done to eliminate the zero crossings and negative amplitudes in the time-domain signal, but the interpolation through the single depth slice leads to introduce irregularity into the image, since the interpolation coefficients differ between the rows in the whole matrix. *Figure (19)* shows the resultant depth slice maps at depth ranging from *0.5 m* to 0.5 *m* in the site. It is clear, regarding anomalous features are visible from 0.5 m depth to 5 m slices. Moreover, these anomalous features, which correspond to the hyperbola seen on the radar sections and interpreted as filled voids. The higher mean amplitude on the slice is related to the soil-bedrock reflection.

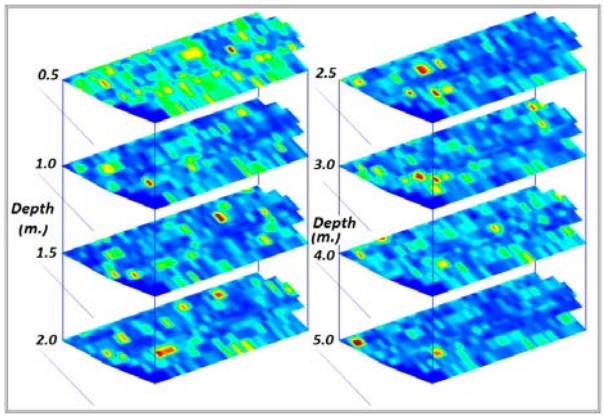

Figure 19: A Series of slices at depth range from 0.5 m to 5 m, shows the lateral lithological changes and air filled voids.

CONCLUSIONS

In the present work, the south Sinai earthquake catalogue is analyzed using *ZMAP software* in order to correlate the seismicity, subsurface structures and seismic sources identification. The hazard reduction, from natural disasters such as earthquakes, becomes a primary concern in south Sinai touristic places especially *(Sharm El-Shikh, Dahab, Nuweiba, Saint Catherine and Ras Mohamed)*, which are moving rapidly towards huge investments and developments. The GPR 2D-cross sections and time slices show that a lot of fractures and sinkholes are associated with the fault system in Sharm El-Sheikh which could be a risk for the buildings. It reveals the branching geometry of the fault and precise location within 1 m.

The interpretation of *TDR* map indicates that the zero contour line will be located at or very close to the *fault / contact*. The predominant directions of the fault systems in south Sinai, through the interpretation of the *TDR* magnetic map has stated: the *NW-SE* direction (Gulf of Suez trend); the *NE-SW* direction (Syrian Arc trend) and *NNE-SSW* (The Gulf of Aqaba trend); the *N-S* direction (East-Africa rift) and the *E-W* direction (Mediterranean Sea trend).

The results indicate that the South Sinai faces hazards as active seismic source zones are located near touristic resorts, which means that catastrophe may be in the near future, as old buildings and non-engineering constructions are abundant in regions. Also, this recommendation is given to decision makers for the high risk that Sharm El-Sheikh suffers. This study is preliminary work on seismicity of south Sinai. Thus, a comprehensive geological and geophysical study is needed to reduce the hazard of earthquakes in the region.

REFERENCES

Abdel Fattah A., Hussein H. and El-Hady S., **2006**. Another look at the 1993. and 1995 Gulf of Aqaba earthquake from the analysis of teleseismic waveforms. Acta Geophysica, 54, 3, 260-279.

Abdel-Rahman K., Al-Amri A., Abdel-Mneim E., **2009**. Seismicity of Sinai Peninsula, Egypt. Arab J. Geoscience. 2, 103–118.

Aboud E., Salem A. and Mekkawi M., **2011**. Curie depth map for Sinai Peninsula, Egypt deduced from the analysis of magnetic data. Tectonophysics, 506, 46–54.

Aboud E., Mekkawi M., Khalil A., Saad U. and Soliman M., **2009**. Reinterpretation of magnetic data of Dahshour area reveals major faults beneath and cross the Nile River, Cairo area. NRIAG Journal of Geophysics, special issue, 211-218.

Agha A., **1981**. Structural map and plate reconstruction of the Gulf of Suez-Sinai area. Conoco Oil, Houston. USA.

Aki K. 1965. Maximum likelihood estimate of b-value in the formula log N= a-bm, and its confidence limits, Bull. Earthquake Res. Inst. 43, 237–239.

Ashami A., 2003. Structural and lithologic controls of uranium and copper mineralization in Um Bogma environs, southwestern Sinai, Egypt, Ph.D. Thesis, Geology Department, Faculty of Science, Mansoura University, Egypt, 134p.

Awad H., Alrifi N., Mekkawi M. and Othman K., **2009**. Subsurface structure and seismicity characteristics of south Sinai area, Egypt. International Journal of Exploration Geophysics, Remote Sensing and Environment (EGRSE), XVI, 9-19.

Badawi A. and Horvath F., **1999**. The Sinai subplate and tectonic evolution of the northern Red Sea region, J. Geodynamics, 27, 443-450

Baer G., Funning G., Shamir G., Wright T., **2008**. The 1995 November 22, Mw 7.2 Gulf of Elat earthquake cycle revisited. Geophys. J. Int., 175, 1040–1054.

Ballard R., **1983**. Cavity detection and delineation research Rep.5, Electromagnetic (radar) techniques applied to cavity detection, Tech. Rep. GL-83-1 U.S. Army Engr. Waterways Expr Station, Viksburg, M.

Batayneh A., Abueladas A. and Moumani, K.,**2002**, Use of ground-penetrating radar for assessment of potential sinkhole conditions: an example from Ghor al Haditha area, Jordan: Environmental Geology, 41, 977-983.

Ben Menahem A., Nur A. and Vered M., **1976**. Tectonics, seismicity, and structure of the afro-Eurasian junction the breaking of an incoherent plate. Phys. Earth planet inter.,12, 1-50.

Ben-Avraham Z., 1985. Structural framework of the Gulf of Elat (Aqaba), Northern Red Sea. Geophys. Res. 90, 703–726.

Colleta B., Le Quellec P., Letouzy J. & Morett, I., **1988**. Longitudinal evolution of the Suez rift structure-Egypt. Tectonophysics, 153, P. 221 – 233.

Conyers, L. B., 1995. The use of ground penetrating radar to map the buried structures and landscape of the Ceren Site, El Salvador. Geoarchaeology, 10, 275-299. **Doolittle, J. A.** and Miller, W. F. **1990.** Geophysical investigations at the Ceren Site, El Salvador. In Sheets, P.D. and Kivit, K. A. (eds), Ceren Project Preliminary Report 1992 (Boulder, Colorado: Department of Anthropology, University of Colorado, 10-19. **EGSMA, 1994**. Egyptian Geological Survey and Mining Authorit, Geologic map of Sharm El-Sheikh, Egypt, 1:25000.

El-Behiry M., and Hanafy, S., **2000**. Geophysical surveys to map vertical extension of a sinkhole: a comparison study, in Powers, M.H., Ibrahim, A.B. and Cramer, L. Proceedings of the Environmental and Engineering Geophysical Society, 341-350.

El-Fiky, G., 2005. GPS-derived Velocity and Crustal Strain Field in the Suez-Sinai Area, Egypt. Bulletin. Earthquakes Research Institute, University of Tokyo, 2, 1-20.

El-Hefnawy, Deif, A., El-Hemamy S. and Gomaa N., **2006**. Probabilistic assessment of earthquake hazard in Sinai in relation to the seismicity in the eastern Mediterranean region. Bull Eng Geol Env, 65: 309–319.

El-Qady, G., Hafez, M., Abdalla, M., and Ushijima, K., **2005**. Imaging subsurface cavities using geoelectric tomography and ground penetrating radar, J. Cave Karst. Stud., 67(3), 174–181,

El-Sayed A., Vaccari F. and Panza G., **2001**. Deterministic seismic hazard in Egypt, Geophys. J. Int. 144, 555–567.

Fergany E., Oth A., and Wenzel F., **2007**. Synthetic of strong ground motion for M = 7.2 earthquake in the Gulf of Aqaba, Sinai-Egypt. NRIAG J. of Geophysics, 6, 81- 95. **Ginzburg A.,** Makris J., Fuches K., Prodehl C., Kaminsky W., Amitai U., **1979.** A seismic study of the crust and upper mantle of the Jordan-Dead Sea rift and their transition toward the Mediterranean Sea. J. Geophys. Res. 84, 1569–1582.

Google Earth website: http://earth.google.com

Ismail A, Sultan A, Mohamady M., **2001**. Bouguer and total magnetic intensity maps of Sinai Peninsula. Scale 1:500,000, Proceedings of the 2nd Int. symposium,hold on Geophysics, Tanta, 111–117.

Korrat I., Hussein H., Marzouk I., Ibrahim E., Abdel-Fattah A. and Hurukawa N. **2006.** Seismicity of the northernmost part of the Red Sea (1995-1999) Acta Geophysica, 54, no. 1, pp. 33-49.

Khafef, A. and & El-Khoudary, S., **2011**. Proprietary of Total Intensity Magnetic Data to Detect the Subsurface Structures and Tectonics of Southern Sinai Peninsula, Egypt. J. of American Science, 7, 3, 453-463.

Lee W. 1990. Hypo71 PC program, IASPEI Software Library, Vol.1.

McClusky A, Reilinger R., Mahmoud S., Beni Sari D. and Tealeb A., **2000**. GPS constraints on Africa (Nubia) ans Arabia plate motions. Geophys. J. Int., 155, 126-138.

Morey R., **1974**, Detection of subsurface cavities by ground penetrating radar: Highway Geological Symposium, Proceedings 27, 28-30.

Neev D., 1975. Tectonic evolution of the Middle East and Levatine basin (easternmost Mediterranean). Geology, 3, 683–686.

Olhoeft G., 1984. Application and limitations of ground penetrating radar: 54th Annual Intrnational Meeting. Society Exploration Geophysics, Expanded Abstracts,147-148.

Olhoeft G., 1988. Selected bibliography on ground penetrating radar: Proc. Of Symposium on Application of Geophysics to Engineers and Environmental problems, Society of Engineers and Mineral Exploration Geophysics, 462-520

Omara S., 1959. The Geology of Sharm El-Sheikh sandstone, Sinai, Egypt. Egyptian Journal of Geology, 3, No. 1.

Patton A., Moustafa R., Nelson N. and Abdine S., **1994**. Tectonic evolution and structural setting of the Suez Rift, in Interior Rift Basins: Tulsa O.

edited by Landon S., Am. Ass. Pet. Geol. Mem., 59, 9-55.

Rabeh T., Miranda J., Carvalho J. and Bocin A., **2009**. Interpretation case study of the Sahl El Qaa area, southern Sinai Peninsula, Egypt. Geophysical Prospecting, 57, 3, 447-459.

Reilinger R., McClusky A., Vernant P., Lawrence S., Ergintav S., Cakmak R., Ozener H., Kadirov F., Guliev E., Stepanyan R., Nadariya M., Hahubia G., Mahmoud S., Sakr K., ArRajehi A., Paradissis D., Al-Aydrus A., Prilepin M., Guseva T., Evren E., Dmitrotsa A., Filikov S., Gomez F., Al-Ghazzi R. and Karam G., **2006**. GPS constraints on continental deformation in the Africa-Arabia-Eurasia continental collision zone and implications for the dynamics of plate interactions. J. Geophys. Res., 111, B05411, 26 PP., doi: 10.1029 / 2005JB004051.

Said R., 1990. The Geology of Egypt, 2nd edition Balkema, Rotterdam, pp 439–449.

Sandmeier, K. J. 2010. Program for Processing and Interpretation of Reflection and Transmission data, Karlsruha, Germany.

Sharp I., Gawthorpe R., Underhill J. & Gupta S., **2000**. Fault-propagation folding in extensional settings: example of structural style and synrift sedimentary response from the Suez rift, Sinai, Egypt. Bull. of Geol. Soc. of America, 112, 12, 1877-1899.

Shamir G., Baer G. and Hofstetter A., **2003**. Three – dimensional elastic earthquake modeling based on integrated seismological and InSAR data: the M_w= 7.2Nuweiba earthquake, Gulf of Aqaba 1995 November. Geophys. J. Int, 154, 731-744.

Steckler M., Berthelot F., Lyberis N., Le Pichon, X., **1988**. Subsidence in the Gulf of Suez: implications from rifting and plate kinematics. Tectonophysics 153, 249–270.

Ulriksen, C.P., **1982**, Application of impulse radar to civil engineering: Ph. D dissertation, Dept. of Engineering Geology, Lund University of Tech, Sweden.

Verduzco B., **2004**. New insights into magnetic derivatives for structural mapping, The Leading Edge, 23, 116-119.

Wadhwa R., Ghosh N., Chandrasekhar V., and Sinharay R., **2008**. Delineation of cavities in a canal by geophysical survey in Navargaon project area, Maharashtra, Journal of Indian Geophysical Union, 12(1), 55–62.

Weimer S., **2001**. A software package to analyze seismicity: ZMAP 6.0, Seism. Res. Lett., 72, 373-382.